

Research Article

TiO₂ Deposition on AZ31 Magnesium Alloy Using Plasma Electrolytic Oxidation

Leon White,¹ Youngmi Koo,¹ Yeoheung Yun,^{1,2} and Jagannathan Sankar¹

¹ Engineering Research Center (ERC), Mechanical Engineering, Department of Chemical, Biological, and Bio Engineering, North Carolina A & T State University, Greensboro, NC 27406, USA

² Engineering Research Center for Revolutionizing Metallic Biomaterials (ERC-RMB), North Carolina A & T State University, 1601 E. Market Street, IRC Room 119, Greensboro, NC 27411, USA

Correspondence should be addressed to Yeoheung Yun; force9488@gmail.com

Received 12 June 2013; Revised 26 November 2013; Accepted 2 December 2013

Academic Editor: Wenhong Fan

Copyright © 2013 Leon White et al. This is an open access article distributed under the Creative Commons Attribution License, which permits unrestricted use, distribution, and reproduction in any medium, provided the original work is properly cited.

Plasma electrolytic oxidation (PEO) has been used in the past as a useful surface treatment technique to improve the anticorrosion properties of Mg alloys by forming protective layer. Coatings were prepared on AZ31 magnesium alloy in phosphate electrolyte with the addition of TiO₂ nanoparticles using plasma electrolytic oxidation (PEO). This present work focuses on developing a TiO₂ functional coating to create a novel electrophotocatalyst while observing the surface morphology, structure, composition, and corrosion resistance of the PEO coating. Microstructural characterization of the coating was investigated by X-ray diffraction (XRD) and scanning electron microscopy (SEM) followed by image analysis and energy dispersive spectroscopy (EDX). The corrosion resistance of the PEO treated samples was evaluated with electrochemical impedance spectroscopy (EIS) and DC polarization tests in 3.5 wt.% NaCl. The XRD pattern shows that the components of the oxide film include Mg from the substrate as well as MgO and Mg₂TiO₄ due to the TiO₂ nanoparticle addition. The results show that the PEO coating with TiO₂ nanoparticles did improve the corrosion resistance when compared to the AZ31 substrate alloy.

1. Introduction

In recent years, magnesium (Mg) and its alloys have attracted great attention for use as structural materials due to their superior properties which include high strength to weight ratio, low density, good electromagnetic shielding, recycling ability, and good machining [1–3]. Unfortunately, Mg and Mg alloys have very poor corrosion resistance which is attributed to the high chemical activity of Mg. The physical and mechanical properties of Mg implants will decrease as the corrosion of the alloy increases and this disadvantage has limited its use in several applications, particularly in aggressive environments [4, 5].

Surface modification in the form of a coating on the base Mg alloy is one of the most effective ways to prevent corrosion. Currently, there are numerous surface treatments that can be used to provide corrosion protection for magnesium alloys which include chromating, phosphating, electroplating, anodization, waxing, and organic coatings [6–8].

Photo catalysis is a reaction that uses light to activate a substance which in turn modifies the rate of the chemical reaction. TiO₂ is a semiconductor material that is well known for its numerous advantages which include high photo catalytic activity, long-term stability, photosensitivity, and antimicrobial properties [9–11]. Although photo catalytic reactions can only occur under UV light, various studies have been conducted in order to improve the catalytic reaction of TiO₂.

Plasma electrolytic oxidation (PEO) is a surface treatment method that is used to form relatively thick, ceramic-like coatings on metals where the coating is developed from the substrate and the electrolyte. The coatings are formed under high voltages where short-lived discharges occur on the substrate surface to develop the corrosion resistant layer. These coatings provide high hardness and can be used at high temperatures, and the coating process is environmentally friendly [12–14]. The electrolyte composition, electrical parameters, and substrate material all affect the coating

surface morphology, structure, and corrosion resistance. Previous studies have determined that the application of bipolar current regimes usually produces a denser PEO coating on Mg alloys when compared to the unipolar mode. When the electrical parameters are controlled during the PEO process, significant reduction of strong discharges can occur and thereby reduce the detrimental effects associated with these discharge events [15–19].

It is well known that the composition of the PEO coatings is strongly dependent on the electrolyte solution composition and oxidation parameters. The PEO coating used in this study used phosphate as an interface layer. Phosphate plays an important role as a binder between Mg (AZ31) substrate and TiO₂ nanoparticles in this PEO coating. This has an application for photoelectrocatalysts due to the stable surface that is generated. There have been several reports by other researchers that focus on the use of phosphate in PEO coatings for Mg and Mg alloys [20–28]. The addition of TiO₂ into the electrolyte solution has been noteworthy due to its possible uses with solar energy [29, 30], air purification [31, 32], photo catalysis [33, 34], and corrosion protection [35–37]. There have been previous reports that nanoparticles that were added into the electrolyte were incorporated into the PEO coating [38–40]. However, there has been very limited study and focus on the influence of the added TiO₂ nanoparticles on the PEO formation process and coating properties. A PEO coating with TiO₂ nanoparticle addition would help to not only improve the corrosion resistance but also develop a photoelectrocatalyst. The present work focuses on the surface morphology and chemical composition of PEO coatings grown on AZ31D magnesium substrates with the addition of TiO₂ nanoparticles in the electrolyte solution.

2. Materials and Methods

2.1. Sample Preparation. Commercial bicrystalline TiO₂ was supplied by Degussa (P25, 80% anatase and 20% rutile) for this study. Die-cast AZ31 Mg alloy with a nominal composition (mass fraction, %) of 3.0 Al, 1.0 Zn, and balance Mg was used. Cylindrical samples were cut from 1.27 cm diameter rod into 3 mm thick pieces. All samples were connected with copper wire on one side and mounted in epoxy resin with the other surface exposed. The exposed surface gave a working area of 0.785 cm². In order to ensure the same surface roughness of different tested samples, the working electrodes were successively polished using 400-grit, 600-grit, 800-grit, 1000-grit, and 1200-grit abrasive paper, using water as a lubricant. Samples were carefully degreased with acetone, rinsed with distilled water, and dried.

2.2. PEO Coating Preparation. AC PEO treatment was conducted in electrolyte solution with treatment parameters of 100 V RMS and 1000 Hz for 5 minutes. The electrolyte solution consisted of 10 g/L NaOH + 6 g/L TiO₂ + 1 g/L NaH₂PO₄·2H₂O which was prepared using deionized water and was continuously stirred by magnetic stirrer during treatment. Pulse waveforms were applied using the ET Systems electronic GmbH power supply. Voltage/current responses

were monitored electronically with use of a Tektronix TDS 2020 oscilloscope. After coating, samples were rinsed with deionized water and dried in warm air. The electrochemical behavior of the anodized samples was then studied in 3.5 wt.% NaCl solution.

2.3. Coating Characterization

2.3.1. Morphology Study. The surface and cross-section morphologies of the coating were observed using scanning electron microscope operated at a voltage of 10 kV and probe current of 10 mA (Hitachi). Elemental composition of the coatings was analyzed using energy dispersive X-ray spectroscopy (EDX).

2.3.2. Phase Analysis. The phases of the coating were determined using X-ray diffraction (XRD) method. The experiments were performed using a commercial X-ray diffractometer (Bruker D8 Tools instrument; $\lambda = 1.5406 \text{ \AA}$, 40 mA, and 40 kV). The scanning range of diffraction angle (2θ) was set between 20° and 80° with steps of 0.02° and step time of 1 s.

2.3.3. Corrosion Behavior. The electrochemical behavior was examined using a Gamry potentiostat and a conventional three-electrode cell, employing a saturated calomel reference electrode (SCE) and platinum counter electrode. The working electrode was the test material, the test solution was 3.5 wt.% NaCl, and testing was conducted at room temperature.

After 5 minutes of immersion (to become stable), electrochemical impedance spectroscopy (EIS) measurements were performed with a frequency range of 1 Hz–1 MHz and a 10 mV peak-to-peak AC excitation. In the DC polarization tests, the scan rate was conducted at a rate of 5 mV/s for –0.50 V to 1.0 V with respect to the open circuit potential. The corrosion current, I_{corr} , in mA·cm^{–2} can be related to the I_{corr} in millimeters/year (mm·y^{–1}) using (1) [41]. Measurements were performed twice to ensure reproducibility of the results:

$$\text{corrosion rate (mm} \cdot \text{y}^{-1}) = \frac{3.28M}{n\rho} i_{\text{corr}}. \quad (1)$$

n is the number of electrons freed by the corrosion reaction; M is the atomic mass of Mg (24.3 g/mol); ρ is the density of Mg (1.74 g/cm³).

The corrosion potential, corrosion current density, and anodic/cathodic Tafel slopes (B_a and B_c) were obtained using Gamry Instrument. Based on the approximate linear polarization at the corrosion potential (E_{corr}), the polarization (R_p) values were determined using the following from [41]:

$$R_p = \frac{B_a \times B_c}{2.3i_{\text{corr}}(B_a + B_c)}. \quad (2)$$

3. Results and Discussions

3.1. Morphology and Microstructure of Coatings. Figure 1 shows the surface morphology of the PEO coated AZ31 substrate after 5 min treatment in phosphate solution with

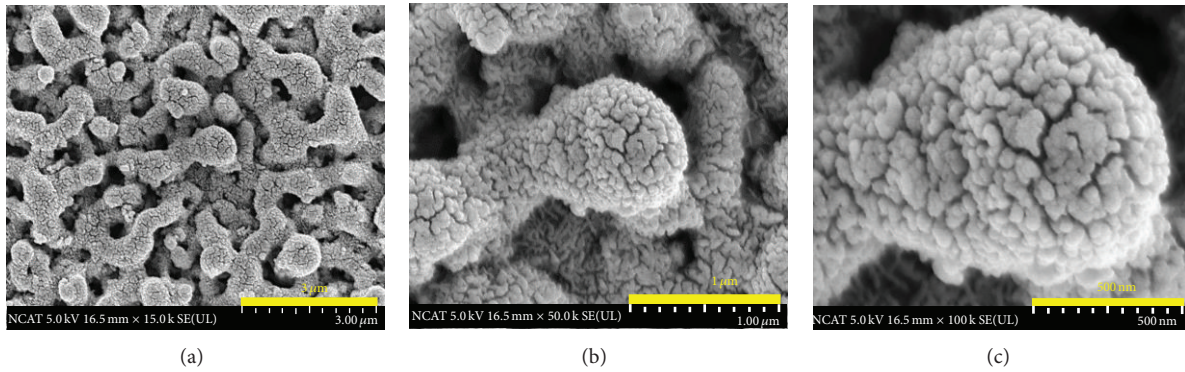


FIGURE 1: PEO coated AZ31 substrate after 5 min treatment in phosphate solution with TiO_2 nanoparticle addition.

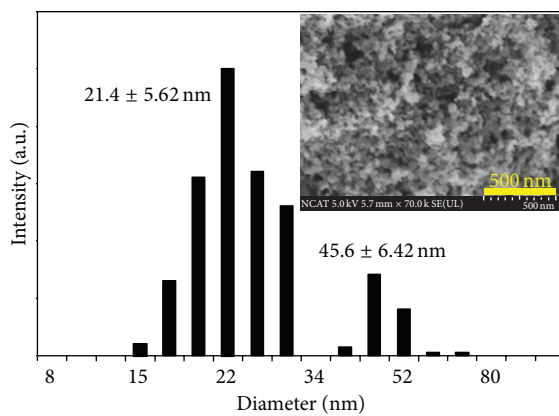


FIGURE 2: Dynamic light scattering data with TiO_2 (inset shows SEM image of TiO_2 particles).

TiO_2 nanoparticle addition. The coating shows the presence of pores which is common for the PEO process [18, 42]. The formation of any PEO coating is based on the sparks passing through the oxide layer and generating discharge tunnels [43]. The observed pores on the surface of the coatings can be reduced in size with optimization, but they cannot be avoided. It is also known that pores grow on the surface with increasing current density. It is clear that the addition of TiO_2 nanoparticles makes a change in the surface morphology of traditional PEO coatings. The SEM images show that the TiO_2 nanoparticles have adhered uniformly to the phosphate layer. Figure 2 shows the size distribution of TiO_2 by dynamic light scattering. The TiO_2 sizes are uniform and are in the size range of 25–40 nm from these results. This size range was also confirmed in other literatures [44–46].

Figure 3 shows the cross-section morphology of the PEO coated AZ31 substrate after 5 min treatment in phosphate solution with TiO_2 nanoparticle addition. The thickness of the coating measured by image analysis from the cross-sections was approximately 2–4 μm . With more cracking and pores, it will be easier for aggressive ions to penetrate the coating and begin to attack the substrate. However, with this cross-section image, there is no sign of major cracking, which helps to improve corrosion resistance. There is no noticeable

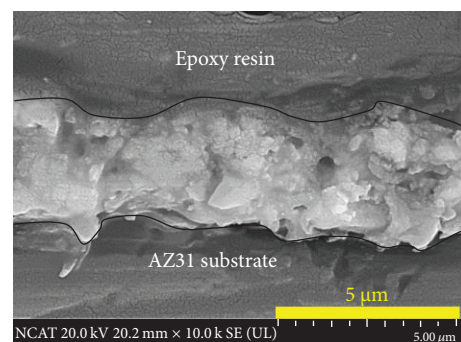


FIGURE 3: Cross-section morphology of the PEO coated AZ31 substrate after 5 min treatment in phosphate solution with TiO_2 nanoparticle addition.

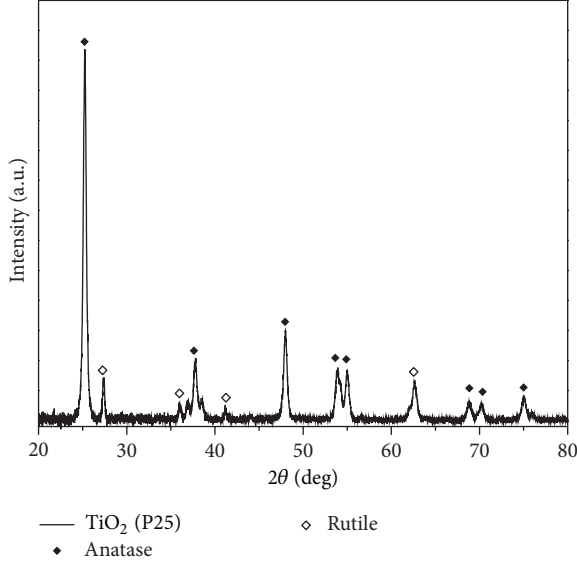
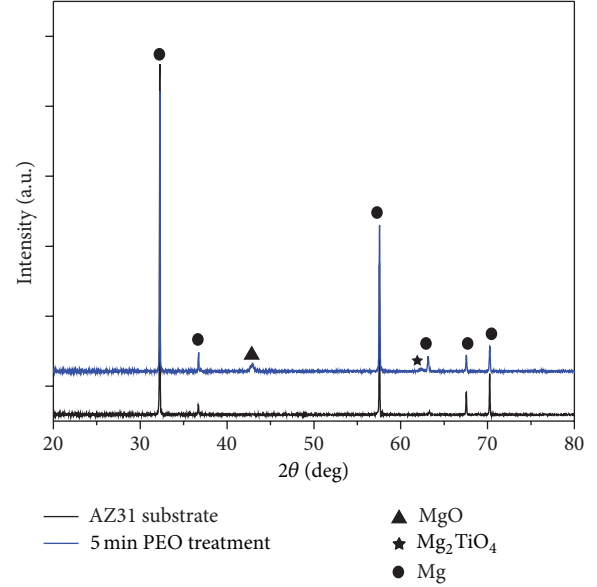
porosity in the layer as the porosity is only on the outer layer close to the surface. The dense/compact structure of the oxide layer also added to the improved corrosion resistance.

3.2. Phase and Chemical Composition. The XRD pattern of the TiO_2 (P25) nanoparticles is presented in Figure 4. It is well known that P25 TiO_2 is a bicrystalline structure and is a mix of anatase and rutile phases. This study used commercial bicrystalline TiO_2 which was supplied by Degussa (P25, 80% anatase, and 20% rutile).

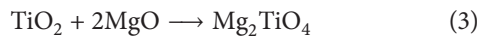
X-ray diffraction (XRD) analysis was used to further investigate the changes in composition of the PEO coatings with addition of TiO_2 nanoparticles in phosphate electrolyte solution. Figure 5 shows the XRD patterns for the AZ31 substrate alloy and PEO coated sample. It can be seen that the AZ31 alloy is mainly composed of a (hcp) magnesium-rich phase. The XRD pattern indicates the presence of a dominating (hcp) magnesium-rich phase, periclase MgO in the coating, and the diffraction peaks assigned to the Mg substrate. The MgO phase was formed when Mg^{2+} cations react with O^{2-} anions under the high temperature and pressure due to the existence of electric field during PEO [43, 47, 48]. The Mg peaks were also observed because through the porosity in the coating the substrate was exposed in a localized manner to the incident X-ray beam. This was also

TABLE I: EDX surface results of PEO coatings formed in phosphate solution with TiO₂ nanoparticle addition.

Coating	Mg	O	Na	P	Ti	Al	Zn
PEO	50.01	46.63	0.26	0.8	1.12	0.89	0.28

FIGURE 4: XRD pattern of TiO₂ (P25) nanoparticles.FIGURE 5: XRD patterns of TiO₂ and PEO coatings formed in phosphate electrolyte with TiO₂ nanoparticle addition.

reported by the other researchers [48, 49]. The low thickness of the PEO film may have also allowed the X-rays to penetrate into the discharge channels and reach the metallic substrate which led to the AZ31 substrate peaks shown. The XRD patterns for the PEO coatings also indicate the presence of Mg₂TiO₄. TiO₂ nanoparticles can participate in the reaction with MgO inside the discharge channel during the PEO process. Mg₂TiO₄ could possibly be formed due to the high temperature in the discharge channels due to the following reaction [50]:



No peaks associated with TiO₂ anatase or rutile phases are detected indicating that these elements may exist in small amounts of crystallized phases and could not be detected. These elements exist in small amounts perhaps due to the short coating time of only five minutes. A longer coating time may allow for the presence of these peaks. Generally, the thicker the oxide layer, the higher the XRD peak intensities [34]. However, it can be concluded that PEO coatings have been produced on AZ31 magnesium alloy in phosphate electrolyte with TiO₂ nanoparticle addition.

The elemental compositions of the PEO coatings were detected by EDX and are listed in Table I. EDX analysis revealed the presence of Mg and O as the major elements of the PEO coating. Elements from the substrate AZ31 which include Al and Zn are found and elements from the electrolyte were also found to include Na, P, and Ti due to TiO₂ nanoparticle addition. The presence of Ti, Na, and P in the coating shows that Na, P, and the TiO₂ nanoparticles are able

to penetrate into the oxide coating during the PEO process. A longer treatment time may show an increased Ti and P content on the surface.

The distributions of chemical elements across the coatings are shown in elemental maps via cross-sections presented in Figure 6. From these maps, it is clear that the major constituents, that is, Mg, O, P, and Ti, are evenly distributed throughout the coating thickness without any distinct irregularities. It is observed that the Ti concentration tends to increase slightly towards the outer region of the coating. Conversely, the P concentration appears to increase at the coating/substrate interface. It can be speculated that the P will deposit first to the substrate due to its strong attraction.

During PEO, the oxide film formation is influenced by plasma microdischarge events which deliver numerous heating-cooling cycles to the surface. These cycles affect the film structure, phase composition, and stress state. A possible explanation for the coating delamination can be found when considering a competition between stress generation and relaxation process during the coating growth [51]. Optimization of the PEO coating parameters (voltage, time, frequency, and current) will help to reduce or eliminate delamination.

3.3. Corrosion Study. The corrosion resistance of the AZ31 substrate and PEO coated AZ31 in phosphate solution with TiO₂ nanoparticle addition was evaluated by the electrochemical polarization test after 5-minute immersion in 3.5 wt.% NaCl solution. This immersion time was so that

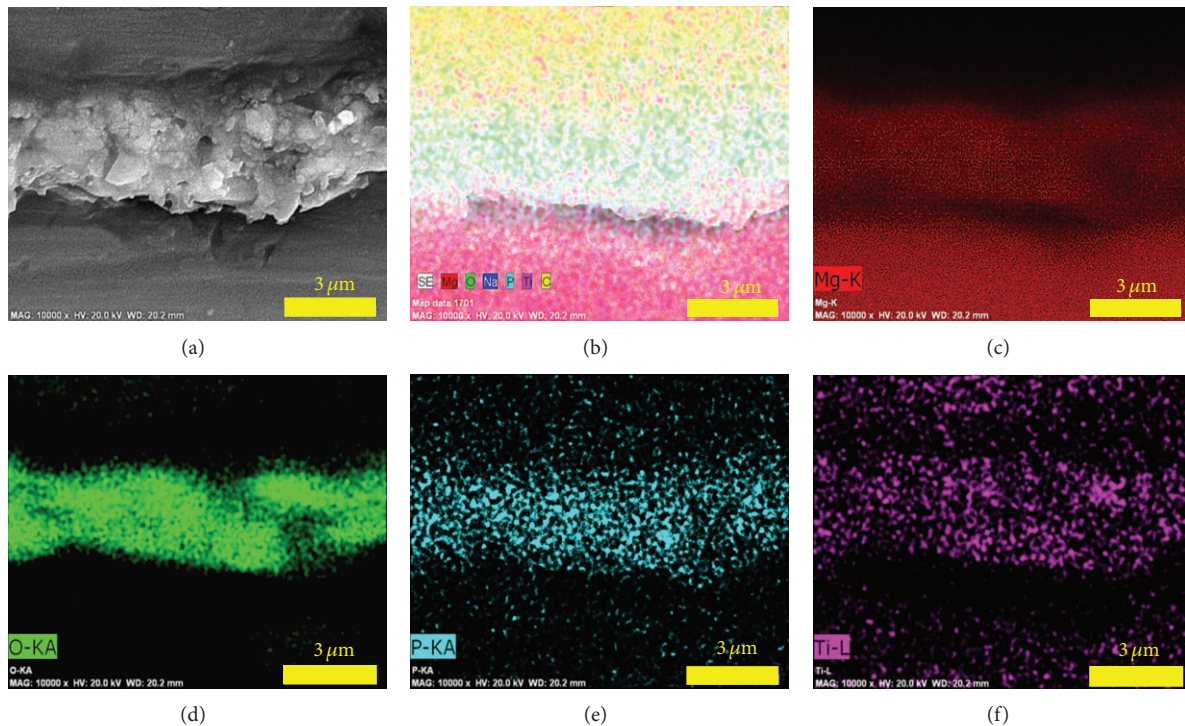


FIGURE 6: EDX elemental maps for coating cross-section of PEO coated sample after 5 min treatment.

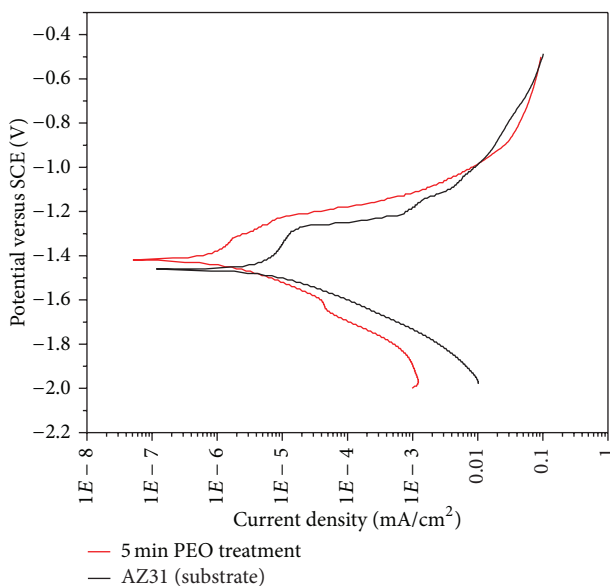


FIGURE 7: Potentiodynamic polarization curves of PEO coated AZ31 and substrate AZ31 in 3.5 wt.% NaCl.

the electrochemical cell could become stabilized. The corrosion potential (E_{corr}) and corrosion current density (I_{corr}) were derived directly from the DC polarization curves.

Figure 7 shows DC polarization curves that compare the uncoated AZ31 sample with the sample coated in phosphate and TiO_2 nanoparticles. This figure shows that the corrosion

resistance of the AZ31 Mg alloy does improve with the use of the PEO treatment for 5 minutes.

Table 2 shows the results from the DC polarization test and gives values for I_{corr} and E_{corr} . Although there was no major change in values of E_{corr} for compared samples (-1.465 V for AZ31 substrate and -1.418 V for PEO coated sample), the values for I_{corr} do show a significant change. The I_{corr} value for the AZ31 substrate sample ($I_{\text{corr}} = 2.45 \times 10^{-3}$ mA/cm²) is three orders of magnitude higher than that for the coated sample ($I_{\text{corr}} = 2.64 \times 10^{-6}$ mA/cm²). This gives way to a much higher corrosion rate when you compare the uncoated AZ31 sample (corrosion rate (mpy) = 5.6×10^{-2}) to the PEO coated sample treated (corrosion rate (mpy) = 6.047×10^{-6}). The remaining corresponding parameters from the polarization curves measuring the corrosion rates are listed in Table 2.

Electrochemical impedance spectrometry (EIS) was carried out for the AZ31 substrate and PEO coated AZ31 as shown in the Nyquist plot in Figure 8. The data in Table 3 shows that the PEO coated sample does offer improvement in resistance with additional R_p and CPE_p values that the uncoated AZ31 sample does not have.

The EIS data for both the uncoated and PEO coated AZ31 samples were fitted with a widely accepted model for coatings (Figure 9) [52, 53]. All the capacitance elements in the equivalent circuit are replaced with the constant phase elements (CPE) in the fitting of the EIS, which is a modified Randles circuit. This model consists of R_s which is the solution resistance. R_p is the outer porous layer resistance and is parallel to the constant phase element (CPE_p). R_b is

TABLE 2: Electrochemical parameters of AZ31 substrate and PEO coating after 5-minute treatment.

Sample	E_{corr} (V)	i_{corr} (A/cm ²)	B_a (V)	B_c (V)	R_p ($\Omega\cdot\text{cm}^2$)	C.R. (mpy)
AZ31	-1.465	2.45×10^{-3}	0.165	0.103	11.25	5.6×10^{-2}
PEO	-1.418	2.64×10^{-6}	0.041	0.074	1.65×10^5	6.047×10^{-6}

TABLE 3: Data of equivalent circuits of AZ31 substrate and PEO coating after 5 minutes.

Sample	R_s ($\Omega\cdot\text{cm}^2$)	R_p ($\Omega\cdot\text{cm}^2$)	CPE _p	R_b ($\Omega\cdot\text{cm}^2$)	CPE _b
AZ31	7.118	204.3×10^{-9}	—	4.02×10^3	293.0×10^{-9}
PEO	15.24	1.114×10^{-6}	3.356×10^{-6}	225.4×10^3	15.57×10^{-6}

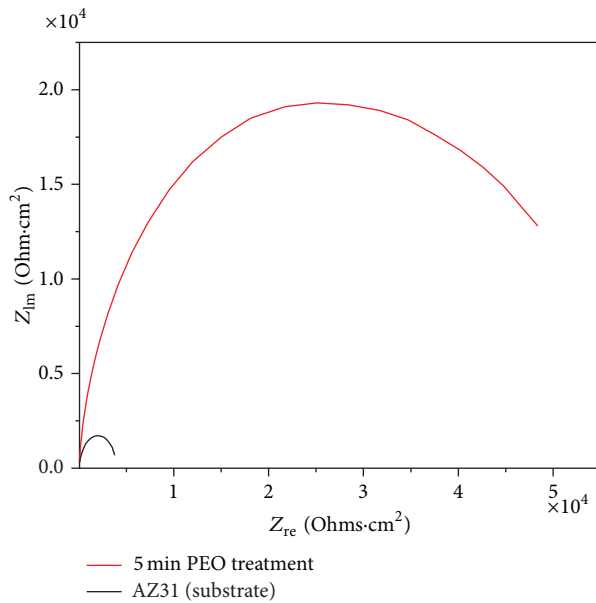


FIGURE 8: Electrochemical impedance curves of PEO coated AZ31 and substrate AZ31 in 3.5 wt.% NaCl.

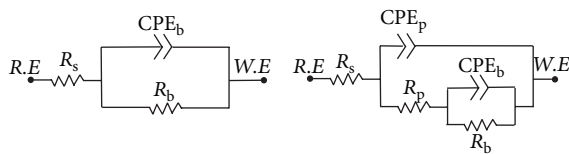


FIGURE 9: Equivalent circuits for fitting the experimental data of (a) AZ31 substrate and (b) PEO coating after 5 min treatment.

inner dense layer resistance paralleled to another constant phase element (CPE_b). The corresponding parameters of fitted equivalent circuits are listed in Table 3. The coating itself does show porosity as shown in Figure 1 which contributed to the low value of R_p . On the other hand, the coating cross-section does show a uniform, relatively dense section. However, a low R_p value and a high R_b value indicate that the porous layer was not able to provide a very high resistance against corrosion. The total resistance of the coating was mainly achieved from the passive layer directly on the metal surface which acted as a barrier against the 3.5 wt.% NaCl to reach the substrate [54].

The SEM images showed a uniform morphology with titanium and phosphorous evenly dispersed. PEO normally shows a porous nature on the surface, but the cross-section images show that there were no signs of major cracking and a compact structure. The XRD analysis proved that Mg₂TiO₄ phase was present in the oxide film which was formed due to the reaction with MgO and TiO₂ nanoparticles in the discharge channels during coating formation. The DC polarization and EIS results showed that the PEO coated AZ31 with phosphate and TiO₂ nanoparticle addition provide increased corrosion resistance when compared to the AZ31 substrate. This can be attributed to the uniform and compact nature of the coating.

4. Conclusions

Oxide film containing TiO₂ compounds was produced on AZ31 magnesium alloy using plasma electrolytic oxidation (PEO) in phosphate electrolyte with the addition of TiO₂ nanoparticles. Further research on photocurrent and photochemical reactions using PEO coated AZ31 substrate with TiO₂ nanoparticles is needed. It will be developed to enhance photo catalytic activity and enable more environmentally-friendly applications.

Acknowledgment

This work was sponsored by the NSF ERC for Revolutionizing Metallic Biomaterials, <http://erc.ncat.edu/>.

References

- [1] B. L. Mordike and T. Ebert, "Magnesium: properties—applications—potential," *Materials Science and Engineering A*, vol. 302, no. 1, pp. 37–45, 2001.
- [2] Y. Zhang, C. Yan, F. Wang, H. Lou, and C. Cao, "Study on the environmentally friendly anodizing of AZ91D magnesium alloy," *Surface and Coatings Technology*, vol. 161, no. 1, pp. 36–43, 2002.
- [3] E. F. Emley, *Principles of Magnesium Technology*, Pergamon Press, Oxford, UK, 1966.
- [4] G. Song, A. Atrens, D. St. John, X. Wu, and J. Nairn, "The anodic dissolution of magnesium in chloride and sulphate solutions," *Corrosion Science*, vol. 39, no. 10-11, pp. 1981–2004, 1997.
- [5] R.-C. Zeng, J. Zhang, W. J. Huang et al., "Review of studies on corrosion of magnesium alloys," *Transactions of Nonferrous*

- Metals Society of China*, vol. 16, supplement 2, pp. s763–s771, 2006.
- [6] G. Song, “Recent progress in corrosion and protection of magnesium alloys,” *Advanced Engineering Materials*, vol. 7, no. 7, pp. 563–586, 2005.
- [7] R. Arrabal, E. Matykina, T. Hashimoto, P. Skeldon, and G. E. Thompson, “Characterization of AC PEO coatings on magnesium alloys,” *Surface and Coatings Technology*, vol. 203, no. 16, pp. 2207–2220, 2009.
- [8] J. E. Gray and B. Luan, “Protective coatings on magnesium and its alloys—a critical review,” *Journal of Alloys and Compounds*, vol. 336, no. 1–2, pp. 88–113, 2002.
- [9] J. Liu, H. Bai, Y. Wang, Z. Liu, X. Zhang, and D. D. Sun, “Self-assembling TiO₂ nanorods on large graphene oxide sheets at a two-phase interface and their anti-recombination in photocatalytic applications,” *Advanced Functional Materials*, vol. 20, no. 23, pp. 4175–4181, 2010.
- [10] L. Armelao, D. Barreca, G. Bottaro et al., “Photocatalytic and antibacterial activity of TiO₂ and Au/TiO₂ nanosystems,” *Nanotechnology*, vol. 18, no. 37, Article ID 375709, 2007.
- [11] M. R. Hoffmann, S. T. Martin, W. Choi, and D. W. Bahnemann, “Environmental applications of semiconductor photocatalysis,” *Chemical Reviews*, vol. 95, no. 1, pp. 69–96, 1995.
- [12] D. Xue, Y. Yun, M. J. Schulz, and V. Shanov, “Corrosion protection of biodegradable magnesium implants using anodization,” *Materials Science and Engineering C*, vol. 31, no. 2, pp. 215–223, 2011.
- [13] R. O. Hussein, D. O. Northwood, and X. Nie, “Coating growth behavior during the plasma electrolytic oxidation process,” *Journal of Vacuum Science & Technology A*, vol. 28, no. 4, pp. 766–773, 2010.
- [14] R. O. Hussein, P. Zhang, X. Nie, Y. Xia, and D. O. Northwood, “The effect of current mode and discharge type on the corrosion resistance of plasma electrolytic oxidation (PEO) coated magnesium alloy AJ62,” *Surface and Coatings Technology*, vol. 206, no. 7, pp. 1990–1997, 2011.
- [15] L. Chang, “Growth regularity of ceramic coating on magnesium alloy by plasma electrolytic oxidation,” *Journal of Alloys and Compounds*, vol. 468, no. 1–2, pp. 462–465, 2009.
- [16] A. L. Yerokhin, L. O. Snizhko, N. L. Gurevina, A. Leyland, A. Pilkington, and A. Matthews, “Discharge characterization in plasma electrolytic oxidation of aluminium,” *Journal of Physics D*, vol. 36, no. 17, pp. 2110–2120, 2003.
- [17] A. L. Yerokhin, A. Shatrov, V. Samsonov et al., “Oxide ceramic coatings on aluminium alloys produced by a pulsed bipolar plasma electrolytic oxidation process,” *Surface and Coatings Technology*, vol. 199, no. 2–3, pp. 150–157, 2005.
- [18] J. A. Curran and T. W. Clyne, “Porosity in plasma electrolytic oxide coatings,” *Acta Materialia*, vol. 54, no. 7, pp. 1985–1993, 2006.
- [19] J. A. Curran and T. W. Clyne, “Thermo-physical properties of plasma electrolytic oxide coatings on aluminium,” *Surface and Coatings Technology*, vol. 199, no. 2–3, pp. 168–176, 2005.
- [20] R. Arrabal, E. Matykina, F. Viejo, P. Skeldon, and G. E. Thompson, “Corrosion resistance of WE43 and AZ91D magnesium alloys with phosphate PEO coatings,” *Corrosion Science*, vol. 50, no. 6, pp. 1744–1752, 2008.
- [21] P. Bala Srinivasan, J. Liang, R. G. Balajee, C. Blawert, M. Störmer, and W. Dietzel, “Effect of pulse frequency on the microstructure, phase composition and corrosion performance of a phosphate-based plasma electrolytic oxidation coated AM50 magnesium alloy,” *Applied Surface Science*, vol. 256, no. 12, pp. 3928–3935, 2010.
- [22] S. Yagi, A. Sengoku, K. Kubota, and E. Matsubara, “Surface modification of ACM522 magnesium alloy by plasma electrolytic oxidation in phosphate electrolyte,” *Corrosion Science*, vol. 57, pp. 74–80, 2012.
- [23] L. Wang, Q. Cai, B. Wei, and Y. Yan, “Analyses of microarc oxidation coating formed on AZ91D alloy in phosphate electrolytes,” *Journal Wuhan University of Technology-Materials Science*, vol. 22, no. 2, pp. 229–233, 2007.
- [24] J. Liang, L. Hu, and J. Hao, “Characterization of microarc oxidation coatings formed on AM60B magnesium alloy in silicate and phosphate electrolytes,” *Applied Surface Science*, vol. 253, no. 10, pp. 4490–4496, 2007.
- [25] Q. Cai, L. Wang, B. Wei, and Q. Liu, “Electrochemical performance of microarc oxidation films formed on AZ91D magnesium alloy in silicate and phosphate electrolytes,” *Surface and Coatings Technology*, vol. 200, no. 12–13, pp. 3727–3733, 2006.
- [26] J. Liang, P. B. Srinivasan, C. Blawert, M. Störmer, and W. Dietzel, “Electrochemical corrosion behaviour of plasma electrolytic oxidation coatings on AM50 magnesium alloy formed in silicate and phosphate based electrolytes,” *Electrochimica Acta*, vol. 54, no. 14, pp. 3842–3850, 2009.
- [27] K. Murakami, M. Hino, M. Hiramatsu et al., “Corrosion protection of AZ91D magnesium alloy by anodization using phosphate electrolyte,” *Materials Transactions*, vol. 48, no. 12, pp. 3101–3108, 2007.
- [28] K. Murakami, M. Hino, and T. Kanadani, *Anodization of Magnesium Alloys Using Phosphate Solution*, InTech, Rijeka, Croatia, 2011.
- [29] H. Chen, W. Li, H. Liu, and L. Zhu, “Performance enhancement of CdS-sensitized TiO₂ mesoporous electrode with two different sizes of CdS nanoparticles,” *Microporous and Mesoporous Materials*, vol. 138, no. 1–3, pp. 235–238, 2011.
- [30] H. Xu, X. Tao, D.-T. Wang, Y.-Z. Zheng, and J.-F. Chen, “Enhanced efficiency in dye-sensitized solar cells based on TiO₂ nanocrystal/nanotube double-layered films,” *Electrochimica Acta*, vol. 55, no. 7, pp. 2280–2285, 2010.
- [31] M.-S. Kim, J.-J. Ryu, and Y.-M. Sung, “One-step approach for nano-crystalline hydroxyapatite coating on titanium via microarc oxidation,” *Electrochemistry Communications*, vol. 9, no. 8, pp. 1886–1891, 2007.
- [32] C. H. Ao and S. C. Lee, “Indoor air purification by photocatalyst TiO₂ immobilized on an activated carbon filter installed in an air cleaner,” *Chemical Engineering Science*, vol. 60, no. 1, pp. 103–109, 2005.
- [33] Y.-K. Shin, W.-S. Chae, Y.-W. Song, and Y.-M. Sung, “Formation of titania photocatalyst films by microarc oxidation of Ti and Ti-6Al-4V alloys,” *Electrochemistry Communications*, vol. 8, no. 3, pp. 465–470, 2006.
- [34] M. R. Bayati, A. Z. Moshfegh, and F. Golestani-Fard, “Effect of electrical parameters on morphology, chemical composition, and photoactivity of the nano-porous titania layers synthesized by pulse-microarc oxidation,” *Electrochimica Acta*, vol. 55, no. 8, pp. 2760–2766, 2010.
- [35] S. V. Lamaka, M. L. Zheludkevich, K. A. Yasakau, R. Serra, S. K. Poznyak, and M. G. S. Ferreira, “Nanoporous titania interlayer as reservoir of corrosion inhibitors for coatings with self-healing ability,” *Progress in Organic Coatings*, vol. 58, no. 2–3, pp. 127–135, 2007.

- [36] S. Sathiyarayanan, S. S. Azim, and G. Venkatachari, "A new corrosion protection coating with polyaniline-TiO₂ composite for steel," *Electrochimica Acta*, vol. 52, no. 5, pp. 2068–2074, 2007.
- [37] G. X. Shen, Y. C. Chen, L. Lin, C. J. Lin, and D. Scantlebury, "Study on a hydrophobic nano-TiO₂ coating and its properties for corrosion protection of metals," *Electrochimica Acta*, vol. 50, no. 25–26, pp. 5083–5089, 2005.
- [38] R. Arrabal, E. Matykina, P. Skeldon, and G. E. Thompson, "Incorporation of zirconia particles into coatings formed on magnesium by plasma electrolytic oxidation," *Journal of Materials Science*, vol. 43, no. 5, pp. 1532–1538, 2008.
- [39] R. Arrabal, E. Matykina, F. Viejo, P. Skeldon, G. E. Thompson, and M. C. Merino, "AC plasma electrolytic oxidation of magnesium with zirconia nanoparticles," *Applied Surface Science*, vol. 254, no. 21, pp. 6937–6942, 2008.
- [40] V. N. Malyshev and K. M. Zorin, "Features of microarc oxidation coatings formation technology in slurry electrolytes," *Applied Surface Science*, vol. 254, no. 5, pp. 1511–1516, 2007.
- [41] D. A. Jones, *Principles and Prevention of Corrosion*, Prentice Hall, Upper Saddle River, NJ, USA, 2nd edition, 1996.
- [42] J. M. Wheeler, C. A. Collier, J. M. Paillard, and J. A. Curran, "Evaluation of micromechanical behaviour of plasma electrolytic oxidation (PEO) coatings on Ti-6Al-4V," *Surface and Coatings Technology*, vol. 204, no. 21–22, pp. 3399–3409, 2010.
- [43] S. Durdu, A. Aytac, and M. Usta, "Characterization and corrosion behavior of ceramic coating on magnesium by micro-arc oxidation," *Journal of Alloys and Compounds*, vol. 509, no. 34, pp. 8601–8606, 2011.
- [44] C. Burda, Y. Lou, X. Chen, A. C. S. Samia, J. Stout, and J. L. Gole, "Enhanced nitrogen doping in TiO₂ nanoparticles," *Nano Letters*, vol. 3, no. 8, pp. 1049–1051, 2003.
- [45] C. Aprile, A. Corma, and H. Garcia, "Enhancement of the photocatalytic activity of TiO₂ through spatial structuring and particle size control: from subnanometric to submillimetric length scale," *Physical Chemistry Chemical Physics*, vol. 10, no. 6, pp. 769–783, 2008.
- [46] J. Jiang, G. Oberdörster, and P. Biswas, "Characterization of size, surface charge, and agglomeration state of nanoparticle dispersions for toxicological studies," *Journal of Nanoparticle Research*, vol. 11, no. 1, pp. 77–89, 2009.
- [47] H. F. Guo, M. Z. An, H. B. Huo, S. Xu, and L. J. Wu, "Microstructure characteristic of ceramic coatings fabricated on magnesium alloys by micro-arc oxidation in alkaline silicate solutions," *Applied Surface Science*, vol. 252, no. 22, pp. 7911–7916, 2006.
- [48] A. Dey, R. U. Rani, H. K. Thota, A. K. Sharma, P. Bandyopadhyay, and A. K. Mukhopadhyay, "Microstructural, corrosion and nanomechanical behaviour of ceramic coatings developed on magnesium AZ31 alloy by micro arc oxidation," *Ceramics International*, vol. 39, no. 3, pp. 3313–3320, 2013.
- [49] P. B. Srinivasan, C. Blawert, M. Störmer, and W. Dietzel, "Characterisation of tribological and corrosion behaviour of plasma electrolytic oxidation coated AM50 magnesium alloy," *Surface Engineering*, vol. 26, no. 5, pp. 340–346, 2010.
- [50] W. Li, M. Tang, L. Zhu, and H. Liu, "Formation of microarc oxidation coatings on magnesium alloy with photocatalytic performance," *Applied Surface Science*, vol. 258, no. 24, pp. 10017–10021, 2012.
- [51] R. H. U. Khan, A. L. Yerokhin, and A. Matthews, "Structural characteristics and residual stresses in oxide films produced on Ti by pulsed unipolar plasma electrolytic oxidation," *Philosophical Magazine*, vol. 88, no. 6, pp. 795–807, 2008.
- [52] S. Sathiyarayanan, S. S. Azim, and G. Venkatachari, "Corrosion resistant properties of polyaniline-acrylic coating on magnesium alloy," *Applied Surface Science*, vol. 253, no. 4, pp. 2113–2117, 2006.
- [53] A. Ghasemi, V. S. Raja, C. Blawert, W. Dietzel, and K. U. Kainer, "Study of the structure and corrosion behavior of PEO coatings on AM50 magnesium alloy by electrochemical impedance spectroscopy," *Surface and Coatings Technology*, vol. 202, no. 15, pp. 3513–3518, 2008.
- [54] A. Ghasemi, V. S. Raja, C. Blawert, W. Dietzel, and K. U. Kainer, "The role of anions in the formation and corrosion resistance of the plasma electrolytic oxidation coatings," *Surface and Coatings Technology*, vol. 204, no. 9–10, pp. 1469–1478, 2010.



Hindawi

Submit your manuscripts at
<http://www.hindawi.com>

